ACS APPLIED MATERIALS & INTERFACES

Research Article

www.acsami.org

Systematic Study of Inherent Antibacterial Properties of Magnesium-based Biomaterials

Hongqing Feng, Guomin Wang, Weihong Jin, Xuming Zhang, Yifan Huang, Ang Gao, Hao Wu, Guosong Wu,* and Paul K. Chu*

Department of Physics and Materials Science, City University of Hong Kong, Tat Chee Avenue, Kowloon, Hong Kong China

ABSTRACT: Magnesium-based materials are preferred in temporary orthopedic implants because of their biodegradability, mechanical properties, and intrinsic antibacterial properties. However, the fundamental mechanism of bacteria killing and roles of various factors are not clearly understood. In this study, we performed a systematic study of the antibacterial properties of two common Mg-based materials using a biofilm forming bacterium. Complete annihilation of the initial 3×10^4 bacteria is achieved with both materials in 0.1 mL LB medium in 24 h, whereas in the control, they proliferate to 10^{10}. The bacteria are killed more effectively in the solution than on the surface, and the bacteria killing efficiency depends more on the concentrations of the magnesium ions and hydroxyl ions than the corrosion rate. The killing process is reproduced using formula solutions, and killing is revealed to stem from the synergetic effects of alkalinity and magnesium ions instead of either one of them or $Mg(OH)_2$ precipitate. Reactive oxygen species (ROS) are detected from the bacteria during the killing process but are not likely produced by the redox reaction directly, because they are detected at least 3 h after the reaction has commenced. The average cell size increases during the killing process, suggesting that the bacteria have difficulty with normal division which also contributes to the reduced bacteria population.

KEYWORDS: *magnesium-based biomaterials, antibacterial properties, alkalinity, magnesium ion release, oxidative stress*

INTRODUCTION

Magnesium alloys are promising materials in medical implants because of their natural biodegradability, favorable elastic modulus, and good biocompatibility.[1−6] Natural degradation of magnesium alloys in the physiological environment produces corrosion products that can inhibit osteoclast-induced osteolysis, promote new bone formation around the implants, and introduce bacterial resistance.[7,8] In particular, the inherent antibacterial properties of Mg alloys are important because bacterial infection is one of the most serious problems after surgery leading to not only implant failure, but also complications, morbidity, and mortality.[9−11] Previous studies have shown that pure Mg and Mg alloys have the intrinsic bacteria killing ability. Nandakumar et al. studied the antibacterial properties of the magnesium alloy AZ31B in a biofilm forming bacteria containing medium and observed that bacteria attachment onto the surface and the total bacteria count increased in the first 2 days but decreased to very low levels on the sixth day.[12] Robinson et al. studied the antibacterial properties of magnesium against three different bacteria and found that the increase in pH and Mg ion concentration did not change with the mass of added Mg and the surviving CFUs of all the three bacteria decreased.[13] Li et al. reported that pure Mg was highly effective against methicillin resistant *Staphylococcus aureus* and observed down expressions of *ica*III and *agr* RNAIII, the encoding genes for several exoproteins and cell surface associated proteins.[14] Lock et al. demonstrated that magnesium alloys decreased the viability and CFU of *Escherichia coli* in a 3 day incubation period in an artificial urine solution.[15] Most of these reports stated that disinfection was caused by alkalinity[13,14] and inactivation was also suggested to stem from degradation of the alloy.[15] All in all, the exact bacteria killing mechanism is still unclear.

In the physiological environment, degradation of Mg and Mg alloys tend to be too fast, giving rise to deleterious effects such as local basicity, excessive hydrogen evolution, and loss of mechanical integrity prior to tissue healing. Therefore, there have been efforts to improve the corrosion resistance by modifying the materials,[16,17] surface,[18−21] and processes.[22,23] In some cases, the corrosion resistance and antibacterial properties can be improved simultaneously, but in other cases, improvement of one is at the expense of the other. For instance, Qin et al. developed a Mg−Nd−Zn−Zr alloy with better antibacterial properties, biocompatibility, and corrosion resistance.[24] Tie et al. produced Ag containing Mg alloys[25] and Ryu et al. deposited a Ag-doped MAO coating on AZ31 alloy with enhanced corrosion and antibacterial resistance.[21] Zhao et al. produced a Zr−O protective film on the surface of two Mg alloys by plasma immersion ion implantation and deposition (PIII&D) and achieved better bacteria repellence.[26] However, He et al. reported that addition of Zn enhanced the antibacterial efficiency at the expense of faster corrosion.[27] Hence, in

Received: February 23, 2016
Accepted: April 4, 2016
Published: April 4, 2016

DOI: 10.1021/acsami.6b02241
ACS Appl. Mater. Interfaces 2016, 8, 9662−9673

order to enhance the performance of Mg-based biomaterials, especially the bacterial resistance, a better understanding of the mechanism is imperative.

Many aspects of the magnesium degradation[28] as shown in reactions 1−5) below may contribute to the bacteria killing efficiency:

$$2H^+ + 2e \rightarrow H_2 \text{ (cathodic partial reaction)} \quad (1)$$

$$2Mg \rightarrow 2Mg^+ + 2e \text{ (anodic partial reaction)} \quad (2)$$

$$2Mg^+ + 2H_2O \rightarrow 2Mg^{2+} + 2OH^- + H_2 \text{ (chemical reaction)} \quad (3)$$

$$2Mg + 2H^+ + 2H_2O \rightarrow 2Mg^{2+} + 2OH^- + 2H_2 \text{ (overall reaction)} \quad (4)$$

$$Mg^{2+} + 2OH^- \rightarrow Mg(OH)_2 \text{ (product formation)} \quad (5)$$

First of all, corrosion occurs at the interface between magnesium and the medium, and so, the surface may be where bacteria killing occurs. For example, for surface-modified stainless steels, the antibacteria ability is limited to the surface but not in the medium.[29,30] Second, the corrosion rates of Mg-based materials differ under different conditions and may affect the efficiency. Third, during corrosion, large amounts of hydroxyl ions and magnesium ions are released into the medium. The high alkalinity itself is a threat to bacteria growth and furthermore, a high magnesium ion concentration may create a high osmotic pressure in the bacteria. Fourth, $Mg(OH)_2$ precipitate is formed and MgO nanoparticles have been reported to have the antibacterial ability.[31,32] All of these factors may contribute to the antibacterial properties to a different degree. However, few studies have heretofore considered all these factors comprehensively. In addition, the volume of a typical magnesium antibacterial assay is several milliliters, making it difficult to compare with other common biometals such as titanium alloys and stainless steels to which 50−100 μl of the medium are usually applied.[33,34]

From the cellular perspective, previous studies are also not thorough. The corrosion process is a redox reaction and so oxidative stress may be caused in the bacteria cells. However, very few studies have been carried out to study the intracellular oxidative stress during corrosion of magnesium. Oxidative stress is an important phenomenon and many effective antibacterial measures cause oxidative stress in bacteria cells, for example, photocatalysis,[35] radiation,[36] H_2O_2,[37] cold plasma,[38] antibiotics,[39] and nanoparticles.[40] Whether oxidative stress is involved in the redox reaction is an interesting question which can better elucidate the relationship between chemical reactions and biological responses. In view of the aforementioned uncertainties concerning the bacteria killing mechanism on Mg and Mg alloys, the roles of the various factors must be better understood. In this work, a systematic study is performed on pure Mg and ZK60 alloy using both 100 μL of the medium in addition to the traditional 1 mL immersion using the biofilm forming bacterium *S. aureus*.

EXPERIMENTAL SECTION

Corrosion Behavior of Mg-based Materials in 0.1 and 1 mL of Medium. Two common magnesium materials, pure magnesium (MG) and ZK60 alloy (Mg−6.0 wt % Zn, 0.5 wt % Zr), were used in this study. The as-cast MG and ZK60 samples were cut into 10 × 10 × 5 mm plates, ground using different successive grades of SiC abrasive paper (up to 1200 grit), ultrasonically cleaned in ethanol for 10 min, and dried. The samples were sealed with silicone rubber to expose a surface area of 10 mm × 10 mm and placed on 24-well plates. One mL of the Luria−Bertani medium (LB medium; 10 g Tryptone, 5 g Yeast extract, and 10 g NaCl in 1 L of distilled water) was added to the wells to immerse the samples or 0.1 mL of the LB was dropped onto the surface of the samples. After corrosion in the 1 and 0.1 mL of the LB medium at 37 °C had occurred for 1, 3, 6, 18, and 24 h, the samples were washed with ethanol and dried. The samples were examined by scanning electron microscopy (SEM, JSM-820, JEOL Ltd., Japan). The leached medium was collected and the pH value and magnesium ion concentration were determined. The pH of the 1 and 0.1 mL LB medium was measured by a mini pH monitor (CLEAN L'EAU PH30, USA) capable of measuring a very small volume of liquid of 30 μL. The leached magnesium ion concentration was determined by inductively coupled plasma optical emission spectroscopy (ICP-OES, PE Optima 2100DV, PerkinElmer, USA). Weight loss measurements were carried out to evaluate the corrosion rate of magnesium alloys. The samples with a surface area of 10 × 10 mm^2 were exposed to 1 or 0.1 mL of the LB medium at 37 °C for 24 h. The corrosion products formed on the surface were removed by immersing the samples in chromic acid (200 g/L CrO3 + 10 g/L AgNO3) for 5 min. Afterward, the samples were rinsed in distilled water and alcohol and dried overnight prior to subsequent measurement. To avoid medium loss from evaporation during the 24 h, the gaps between the wells were filled with autoclaved distilled water and this step was critical in the 0.1 mL experiment. If the gaps were not filled with water, the 0.1 mL LB medium would evaporate after 24 h, but if they were filled with water, as much as 90 μl of the LB medium could be recollected after 6 h and 50−60 μL recollected even after 24 h.

Antibacterial Property of Mg-based Materials in 0.1 and 1 mL Medium. The biofilm forming bacteria *Staphylococcus aureus* (ATCC 29213) were used to evaluate the disinfection ability of the magnesium materials. The bacteria in frozen stock were cultured in LB medium at 37 °C and 220 rpm overnight, diluted to OD_{600} = 0.10, and cultured for an additional 1 h to OD_{600} = 0.2 (1.5 × 10^9 /mL). In the 1 mL experiments, the bacteria were diluted 50 000 folds with the LB medium and 1 mL of it was placed in the well containing the Mg samples. In the 0.1 mL experiments, the bacteria were diluted 5000 times with the LB medium and 0.1 mL of it was dropped on the sample surface. The total amount of bacteria was 3 × 10^4 colony forming units (CFU) initially in both sets of experiments. Again, to avoid medium loss due to evaporation, the gaps between the wells were filled with autoclaved distilled water. At time points of 1, 3, 6, 18, and 24 h, the bacteria were collected, serially diluted by 10-fold, and spread on LB agar to perform CFU counting after culturing for 12 h. In the 24 h experiments, the 0.1 mL of the culture liquid was spread on agar without dilution or recultured with 10 mL of fresh LB to check whether there were any living CFUs. The control sample was polystyrene with the bacteria cultured on the surface on 24 well plates in pure LB. The morphology of the 3 × 10^4 CFU in 1 or 0.1 mL of the LB medium after 24 h at 37 °C was observed by SEM. Furthermore, 3 × 10^7 CFU in 0.1 mL of the LB medium were put on the MG and ZK60 samples and incubated at 37 °C for 24 h for observation. After getting rid of the bacteria medium and washing with PBS, the magnesium samples with bacteria on the surface were fixed with 4% paraformaldehyde for 10 min and immersed in a series of ethanol solutions (25, 50, 75, 90, 95, and 100 v/v %) for 5 min sequentially. The samples were dried at 37 °C for 1 day prior to observation by scanning electron microscopy (SEM, JSM-820, JEOL Ltd., Japan). Titanium plates, which had no bacteria killing ability,[34] were assessed as the control.

Disinfection Efficiency of M(*a*)-P(9.5) and M(*a*)-P(9.0) Formula Solutions. To investigate the roles of leached Mg ions and alkalinity during the inactivation process, formula solutions M(*a*)-P(9.5) and M(*a*)-P(9.0) were prepared. The solutions were autoclaved after preparation or made from autoclaved solutions to avoid bacterial contamination. M(*a*) means that the LB medium was added with $MgCl_2 \cdot 6H_2O$ to achieve a Mg^{2+} concentration of *a* × 100 ppm (for

DOI: 10.1021/acsami.6b02241
ACS Appl. Mater. Interfaces 2016, 8, 9662−9673

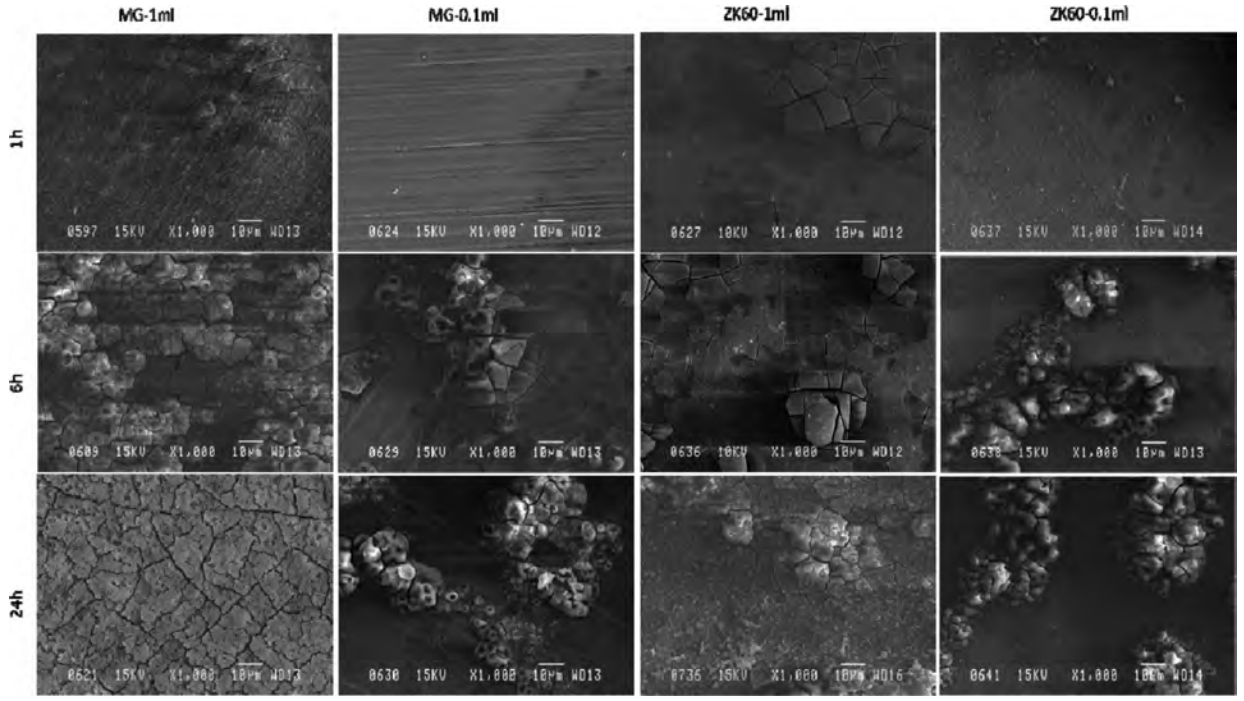

Figure 1. Surface morphology by SEM after corrosion in 1 and 0.1 mL of the LB medium.

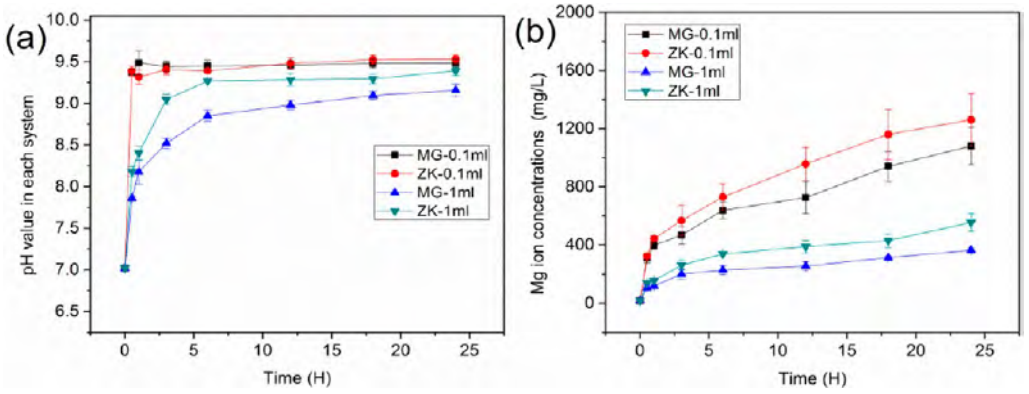

Figure 2. (a) pH value and (b) leached magnesium ion concentration in the experiments involving 1 and 0.1 mL of the LB medium.

example, M(3) means that the Mg2+ concentration was 300 ppm). They were modified with 1 M NaOH to get a pH of 9.7. The solutions were maintained in 1.5 mL Eppendorf tubes during the 24 h bacteria killing experiment and referred to as M(a)-P(9.5), because the pH dropped to 9.5 within 3 h and became steady afterward during 24 h. The pH drop was due to the interaction between the solution and carbon dioxide and oxygen in air. Some $Mg(OH)_2$ precipitates formed at the high pH. The influence of the $Mg(OH)_2$ precipitate on the bacteria killing process was investigated by centrifuging. The CFU curves of the solutions containing $Mg(OH)_2$ (M(a)-P(9.5)(+)) or not containing $Mg(OH)_2$ (M(a)-P(9.5)(−)) were compared. The M(a)-P(9.7) solutions were maintained on 24-well plates, where the interactions between the solution and air were more than those in the tubes, but the same as those on the magnesium plates. The pH dropped to 9.0 in the first 3 h and stabilized afterward. It was referred to as M(a)-P(9.0). The antibacterial ability of the M(a)-P(9.0) solutions were measured and compared with that of the M(a)-P(9.5) solutions. The *S. aureus* bacteria were cultured as aforementioned. Three $\times 10^4$ CFU were treated with 0.1 mL of the M(a)-P(b) solutions for 1, 3, 6, 18, and 24 h and the remaining CFUs were counted to evaluate the antibacterial ability.

Bacteria Cellular Response to Mg-based Materials and M(a)-P(9.5) Solutions. The cell size change and reactive oxygen species (ROS) production in the *S. aureus* bacteria cells were evaluated using flow cytometry. To obtain better results on the cytometry instrument, 10^7 bacteria were used. The cell size was evaluated according to the forward-scattered light (FFS) signals of flow cytometry and ROS was detected using 2′,7′-dichlorodihydrofluorescein diacetate (H_2DCFDA, Life Technologies, Carlsbad, CA). The bacteria cells were collected at specific time points, washed with PBS, and incubated in H_2DCFDA containing PBS (10 μM) at 37 °C for 15 min. The cells were then washed with PBS, resuspended in 0.5 mL of PBS, and determined by flow cytometry with Ex/Em: 488/525 nm.

Statistical Analysis. Each experiment was repeated at least 3 times and the results were shown as mean (average) ± SD (standard deviation). Any significant difference was determined by the T-Test.

RESULTS

Corrosion Behavior. SEM shows that immersion in 1 mL of the medium produces more severe corrosion than contact with 0.1 mL of the medium. As shown in Figure 1, after 1 h, cracks appear from the surface of MG and ZK60 in 1 mL of the medium, but the sample with 0.1 mL of the medium introduced to the surface is still smooth only showing a thin layer of corrosion products. After 6 h, the surface of the 1 mL sample

DOI: 10.1021/acsami.6b02241
ACS Appl. Mater. Interfaces 2016, 8, 9662−9673

exhibits larger and denser cracks with white corrosion products accumulated on the broken surface making the surface quite rough. In comparison, corrosion cracks and broken points are only observed from some spots on the 0.1 mL sample. After 24 h, the 1 mL sample is covered by a thick layer of corrosion products with large and deep cracks. For the 0.1 mL samples, corrosion develops further for more than 6 h, but the broken spots are still parts of the surface.

The pH values and leached Mg ion concentrations are shown in Figure 2. The pH of the 0.1 mL medium reaches 9.5 in 0.5 h and stabilizes afterward. With regard to the 1 mL sample, the pH increase is slower. The pH continues to increase in the first 6 h and then stabilizes. The final stable pH is 9.0 for MG and 9.25 for ZK60. The magnesium ion concentrations also exhibit different trends in the two sets of experiments. With regard to the 0.1 mL sample, the magnesium ion concentration is 1200 mg/L after 24 h whereas it is 400 mg/L for the 1 mL sample. However, although both the hydroxyl and magnesium ion concentrations are smaller in the 1 mL than 0.L mL samples, the total amounts of hydroxyl and magnesium ions produced by corrosion are larger in 1 mL than 0.1 mL, because the total amount is concentration × volume. The ion concentrations in the 1 mL sample are much more than 1/10 of those of the 0.1 mL sample and so the total amounts of released hydroxyl and magnesium ions in 1 mL are larger than those in 0.1 mL. This is consistent with the SEM images in Figure 1.

The corrosion rates are measured by weight losses. As shown in Figure 3, the corrosion rates of the 0.1 mL samples are less

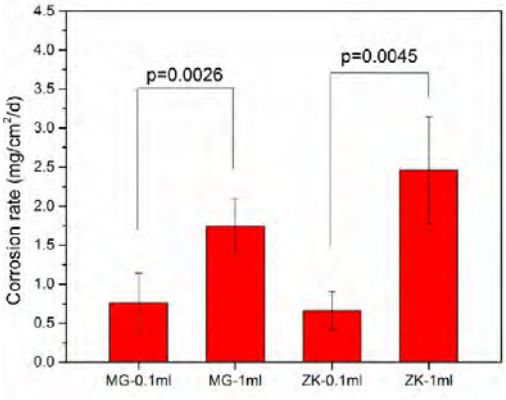

Figure 3. Corrosion rates of the samples in 1 and 0.1 mL of the LB medium determined by weight losses.

than 0.75 mg/cm^2/d, but those of the 1 mL samples are more than 2 mg/cm^2/d, and the differences are significant for both MG and ZK60. The corrosion rates of the 1 mL samples for both MG and ZK60 are larger than those of the 0.1 mL samples, in agreement with the SEM images and Mg concentrations.

Figures 1−3 suggest that corrosion of the Mg materials takes place faster and more severely in 1 mL medium than 0.1 mL medium. This is reasonable because the medium with a large volume can take up more Mg ions and hydroxyl ions, whereas a smaller volume gets saturated more easily, thus slowing the corrosion rate.

CFU Counts. The antibacterial efficiency is quite different for the 0.1 and 1 mL samples, as shown in Figure 4. In the 0.1 mL medium, reduction of CFUs starts within 1 h. The population of the *S. aureus* bacteria continues to diminish

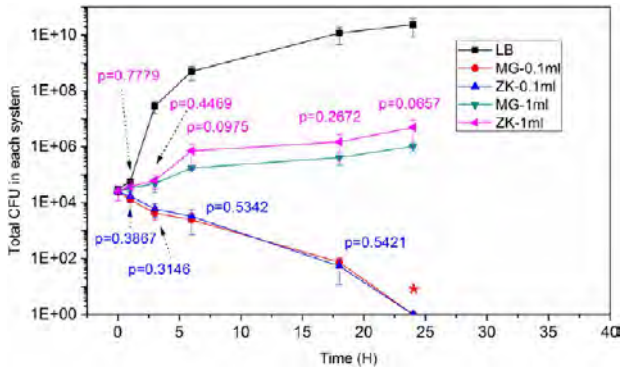

Figure 4. Twenty-four-hour CFU curves of *S. aureus* of the Mg-based samples in 1 and 0.1 mL of the LB medium. The p-value at each time point is marked in the figure; (purple) 1 mL and (blue) 0.1 mL.

during 24 h and at the end, no live bacteria can be observed from either the solid LB agar plate or liquid LB medium (indicated by a red asterisk). The CFUs at each time point are very similar for MG and ZK60. In the 1 mL experiments, the bacteria actually proliferate initially albeit at a smaller rate. In the first 3 h, the growth rate is slow, but from 3 to 6 h, there is exponential growth. After 6 h, the bacteria go to the stationary phase and the final CFUs for the 1 mL samples are about 10^6 after 24 h. The CFUs of ZK60 are more than those of MG after 6 h, but there is no significant difference between the two materials. With regard to the control, the bacteria enter the exponential phase after 1 h and the final total CFUs are more than 10^{10} after 24 h.

Morphology of Bacteria. The 3×10^4 bacteria on the samples are observed by SEM. No bacteria can be found on both the MG and ZK 60 samples in 1 mL medium after 1, 3, and 6 h. After 18 h (Figure 5), dead (dashed arrows) and live cells coexist on MG and ZK60. After 24 h, more bacteria can be found from the samples; many of the bacteria have irregular or broken morphology, suggesting they are dead (dashed arrows). The bacteria attach loosely to the surface due to sedimentation rather than physical adhesion. In contrast, the bacteria adhere tightly on the Ti surface and form a dense biofilm.

In the 0.1 mL experiments, if the initial amount is 3×10^4 CFU, no bacteria can be found by SEM during the whole 24 h and so the initial amount is raised to 3×10^7. In the latter case, some bacteria can be found, and 3×10^7 bacteria growth is also observed from Ti (Figure 6). After 1 h, more than 10 times the number of bacteria are found from Ti than from MG or ZK60. After 3 h, more bacteria are found in small, loose clusters on MG and ZK60 but those on Ti adhere tightly in a large number. After 6 h, the amounts of bacteria on MG and ZK60 decrease. They attach loosely and dead ones (dashed arrows) become visible. These results suggest that during incubation, the bacteria have very limited contact with the sample surface and killing occurs predominantly in the solution rather than on the surface.

CFUs in M(*a*)-P(9.5) Solutions. The killing effectiveness rendered by magnesium ions and alkalinity (pH 9.5) individually and in combination is shown in Figure 7. The M(12) solution hardly causes any difference in bacteria proliferation in the first 6 h. Afterward, there is a small decrease in the cell number in M(12) than LB, but the cells still proliferate more than 5×10^9 in 0.1 mL of the solution. It suggests that a high concentration of magnesium ions has almost no bacteria killing ability. The M(0)-P(9.5) solution

DOI: 10.1021/acsami.6b02241
ACS Appl. Mater. Interfaces 2016, 8, 9662−9673

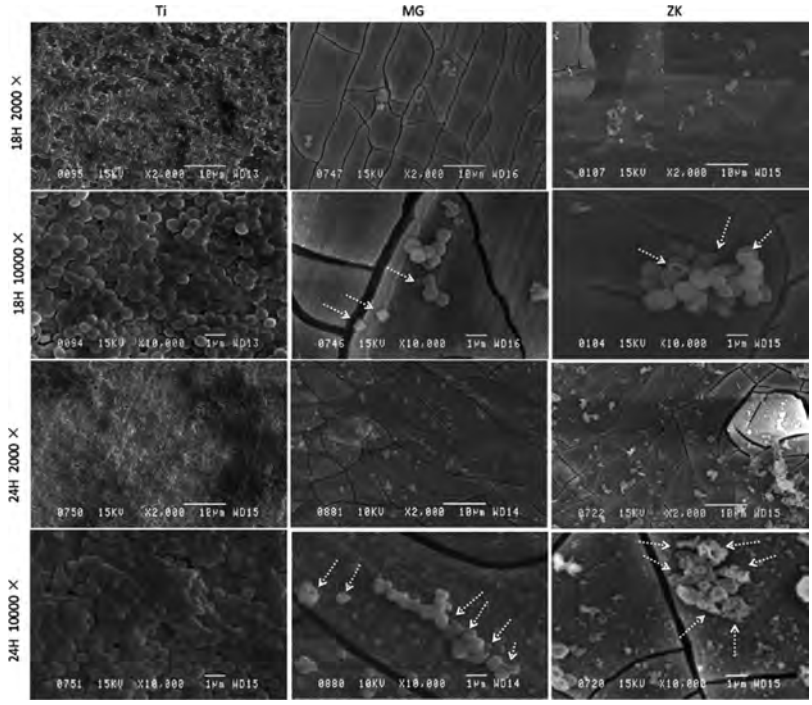

Figure 5. Morphology of the adhered bacteria on the samples in the 1 mL experiments (CFU = 3×10^4 at 0 h); dead cells are indicated by dashed arrows.

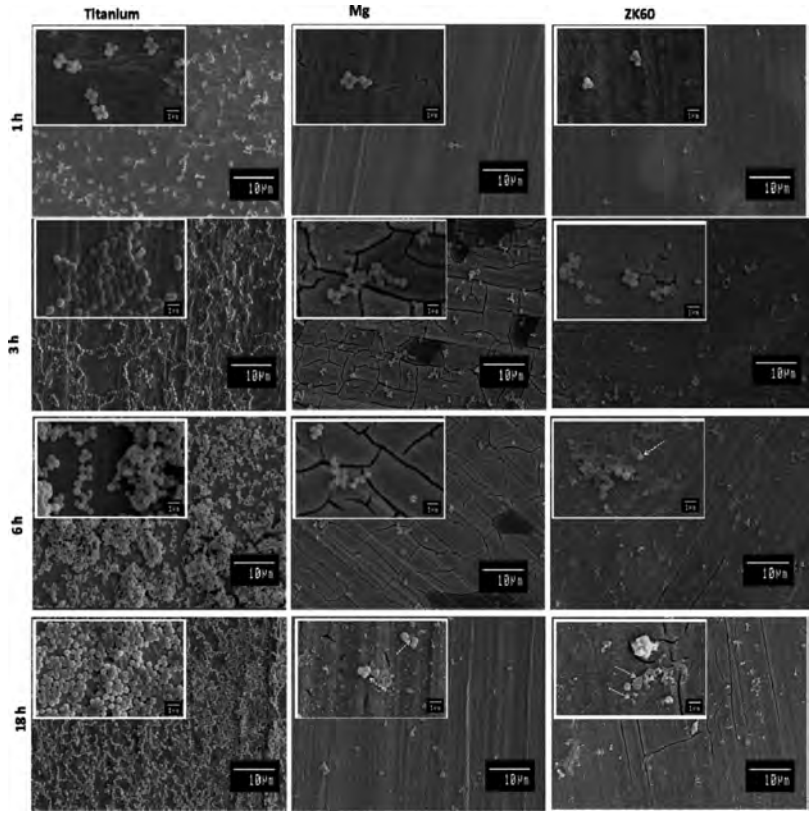

Figure 6. Morphology of the bacteria on the samples in the 0.1 mL experiments (CFU = 3×10^7 at 0 h); dead cells are indicated by dashed arrows.

shows some growth inhibition, especially in the first 3 h, but the cells begin to grow exponentially after 6 h, albeit at a slower rate compared to LB. After 24 h, the cell number is about 8×10^6 suggesting that the final pH resulting from magnesium leaching alone does not play a significant role in bacteria inactivation. On the contrary, the combination of Mg leaching and alkalinity gives rise to complete killing of the bacteria. The solution M(12)-P(9.5) shows even faster killing as demonstrated by complete killing (indicated with *) after only 18 h. The alkaline solutions with a smaller Mg concentration, M (6)-P (9.5) and

DOI: 10.1021/acsami.6b02241
ACS Appl. Mater. Interfaces 2016, 8, 9662−9673

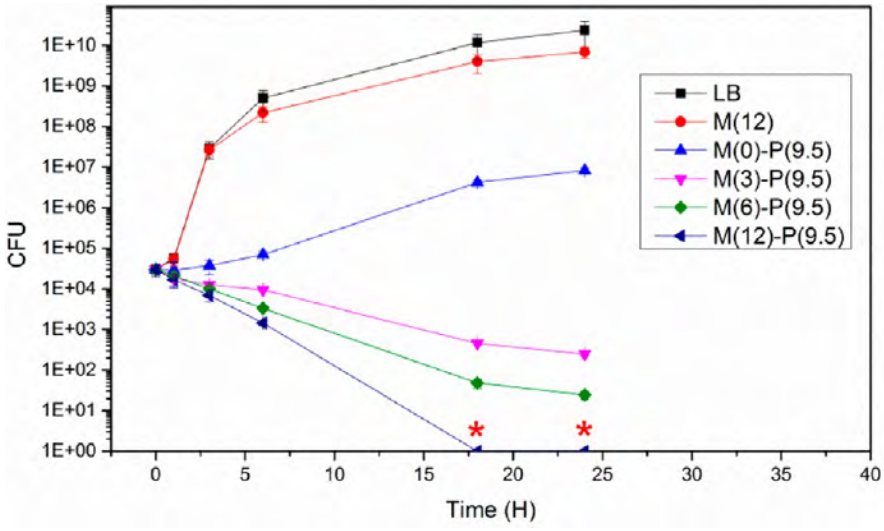

Figure 7. Antibacterial ability of Mg ions and alkalinity alone and in combination.

M (3)-P (9.5), also exhibit a steady decline in the bacteria numbers with time.

CFUs in M(*a*)-P(9.5) Solutions with or without Mg-(OH)$_2$ Precipitate. During the preparation of the M($a > 0$)-P(9.5) solutions, Mg(OH)$_2$ precipitates are observed. To evaluate whether these Mg(OH)$_2$ precipitates contribute to bacteria killing, they are removed from the solutions by centrifuging. The killing efficiency of solutions without Mg(OH)$_2$ precipitates (M(a)-P(9.5)(−)) are compared with ones containing Mg(OH)$_2$ precipitates (M(a)-P(9.5)(+)) as shown in Figure 8. The remaining CFUs of the M(a)-

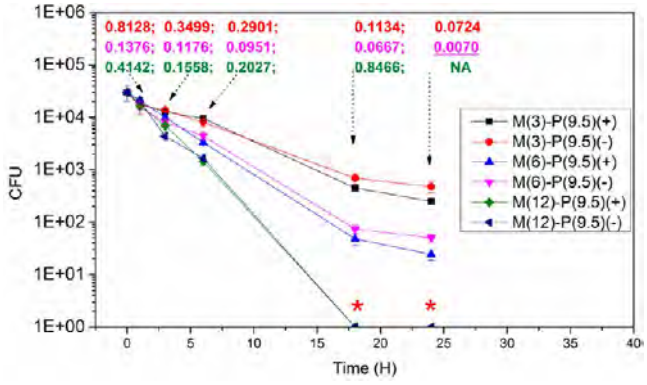

Figure 8. Remaining CFUs in the M(a)-P(9.5) solutions with or without Mg(OH)2 precipitates. The p-value of the statistical analysis of each group at each time point is listed in the figure; (red) M(3)-P(9.5); (purple) M(6)-P(9.5); (green) M(12)-P(9.5); (NA) not applicable; and $p < 0.05$ is underlined.

P(9.5)(−) solutions at each time points from 1 to 24 h are very close to the respective M(a)-P(9.5) (+) solutions. There are no significant differences according to t test for all the pairs, except for the M(6)-P(9.5) group at 24 h, when there were less surviving CFU in the M(6)-P(9.5)(−) solution than M(6)-P(9.5)(+) solution. As a result, the Mg(OH)$_2$ precipitates do not have a big impact on bacteria killing or contribute to the mechanism.

CFUs of Bacteria in M(*a*)-P(9.0) Solutions. Contact with oxygen and carbon dioxide decreases the pH of the solutions as shown in Figure 9. The M(a)-P(9.5) solutions are kept in tubes

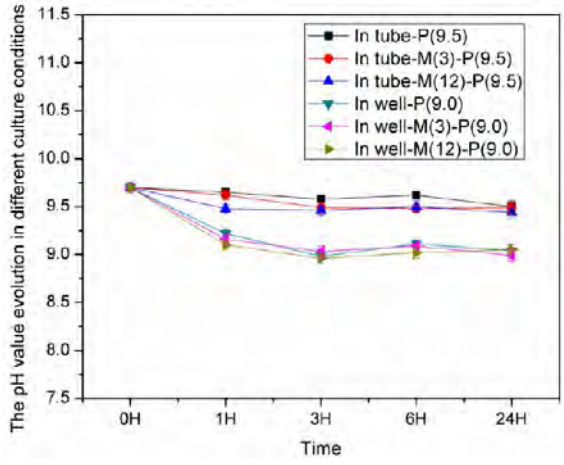

Figure 9. pH evolution in the M(a)-P(9.7) solutions in the tubes and wells.

during the experiments, and the pH drops from 9.7 to 9.5 in the first 3 h before stabilizing. In comparison, the pH of the solutions on the 24-well plate for both MG and ZK60 decreases to 9.0 before stabilizing. The CFU curves of bacteria cultured in M(a)-P(9.0) are shown in Figure 10. When the pH drops by 0.5, the killing ability in the M(0)-P(9.0) solution diminishes. The bacteria grow faster during the exponential phase and the final CFU is more than 10^9 that is 3 orders of magnitude larger than that observed from M(0)-P(9.5). However, when magnesium ions are present, the decrease in the bacteria killing ability is much smaller. M(12)-P(9.0) can annihilate the bacteria at 24 h, 6 h later than M(12)-P(9.5). The final CFUs for M(6)-P(9.0) and M(3)-P(9.0) after 24 h are about 1 order of magnitude larger than those for their respective P(9.5) solutions. In general, in the M($a > 0$)-P(9.0) solutions, the bacteria population declines with time in spite of lower efficiency.

Cellular Response on Mg. Magnesium corrosion is a redox reaction and it is important to identify the formation of ROS in the bacteria and the role in the killing process. The bacteria cultured on MG and ZK60 in the 0.1 mL medium are collected, stained, and analyzed for ROS by flow cytometry (Figure 11). After 1 h, the fluorescent intensity of MG and

DOI: 10.1021/acsami.6b02241
ACS Appl. Mater. Interfaces 2016, 8, 9662−9673

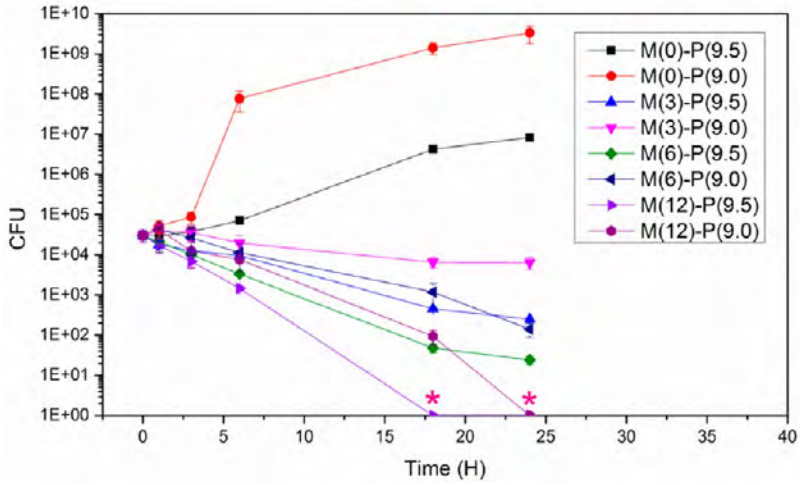

Figure 10. Remaining CFUs in the M(*a*)-P(9.0) solutions in comparison with M(a)-P(9.5).

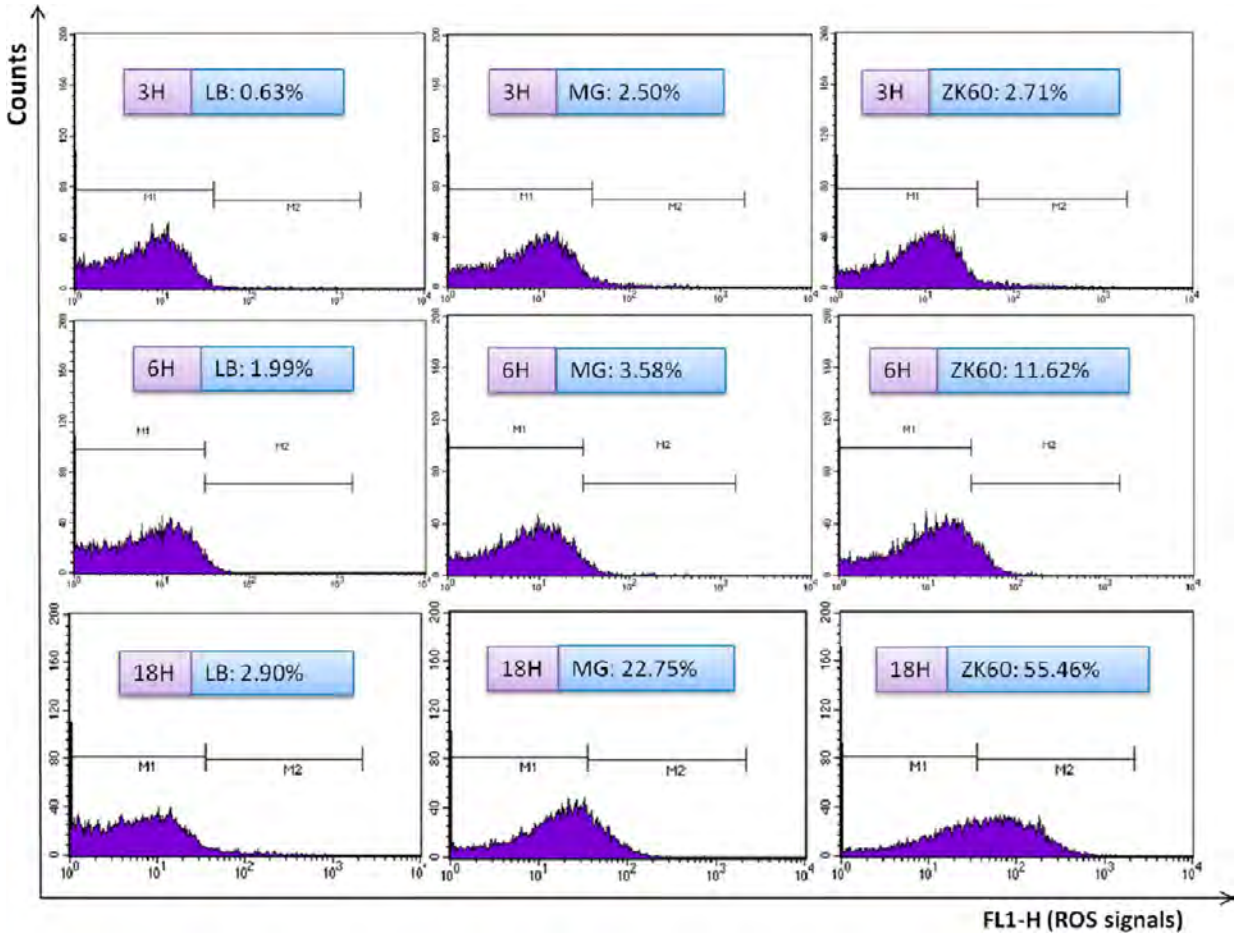

Figure 11. ROS signals detected from the bacteria in the 0.1 mL experiments for MG and ZK60.

ZK60 is the same as that of the pure LB medium and untreated control. After 3 h, the ROS positive cells increase a little bit to 2% as shown in Figure 11. After 6 h, 4−12% ROS positive cell are indentified. After 18 h, they increase further to 20−50% with the curves moving largely to the right side. The time-dependent ROS signals suggest that the ROS are unlikely to be produced directly by the redox reaction. The reaction is faster in the beginning and slows down gradually afterward in contrary to the tendency observed from the ROS signals.

Flow cytometry is used to disclose the cell size by monitoring the FSC signals (Figure 12). The cell size is an important factor for bacteria cell division.[41] Normal cells undergo division for a large enough size, and it stops if the size is too small. The average cell size of the control (LB) becomes smaller with culturing time and it is in agreement with the larger proliferation rate (exponential phase) in the beginning and the small rate at the stationary phase. After 1 h, the average cell sizes of the treated and untreated bacteria are similar, but after

DOI: 10.1021/acsami.6b02241
ACS Appl. Mater. Interfaces 2016, 8, 9662−9673

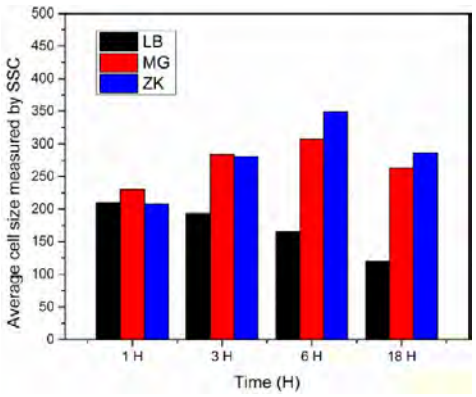

Figure 12. Average cell size of the bacteria cultured in pure LB (control) and 0.1 mL of the medium for MG and ZK60.

3 h, obvious cell size expansion is detected from the Mg samples. During the subsequent 21 h, the cells continue to become bigger compared to the control (LB). The increase in the average cell size compared to the respective control is about 50, 100, and 120% after 3, 6, and 18 h. This cell size expansion induced by Mg most likely indicates that the bacteria have difficulty doing normal division, which may be another factor of the reduced bacteria population in addition to direct cell death caused by magnesium.

Cellular Response in Fomula Solutions. To determine whether the M(a)-P(9.5) solutions can cause similar bacteria cellular response, the cell size and ROS signals with bacteria in the solutions are assessed. Not only can the M(a)-P(9.5) solutions produce killing curves of bacteria, they can also cause the same temporal response in the bacteria. As shown in Figure 13, after 3 h, the M(12) solution shows an average cell size similar to that of the untreated control in pure LB and M(0)-P(9.5) show a small increase in the cell size. However, the M(a > 0)-P(9.5) solutions show obvious cell size enlargement of 40% ∼ 60%, similar to that observed from MG and ZK60 in the 0.1 mL experiments. In addition, ROS positive cells are found from the M(a > 0)-P(9.5) solutions as shown in Figure 14. About 10−25% of the ROS positive cells are in the M(a > 0)-P(9.5) solutions. The M(12) solution does not produce ROS positive cells and the M(0)-P(9.5) solution only produces 2% positive cells. The M(a > 0)-P(9.0) solutions induce the cellular response at the respective time points albeit weaker than M(a > 0)-P(9.5) (data not shown).

DISCUSSION

Contribution of Various Killing Mechanisms. The bacteria killing process and mechanism on Mg are investigated. We first compare Mg corrosion and bacteria killing in 1 mL (immersion) and 0.1 mL (dropping) of the medium. Formula solutions containing hydroxyl ions, magnesium, and $Mg(OH)_2$ precipitate are prepared to analyze the various factors and the cellular response including oxidative stress and the cell size change is monitored.

As summarized in Figure 15, the corrosion rate/weight loss, surface, redox reaction occurring on the surface, magnesium hydroxide precipitate, and magnesium ions are excluded from the critical factors individually. First of all, in our experiments with two medium volumes, the 0.1 mL ones show slower corrosion than the 1 mL one, but the bacteria killing efficiency of 0.1 mL is higher. Second, the bacteria hardly adhere to the surface during the killing process, and the intracellular ROS signals do not show in the beginning when the reaction is fastest, but 3−6 h later. These observations suggest that bacteria are not killed on the surface of the Mg. Third, the M(a)-P(9.5) and M(a)-P(9.0) solutions with different pH and magnesium ion concentrations are prepared and used in our

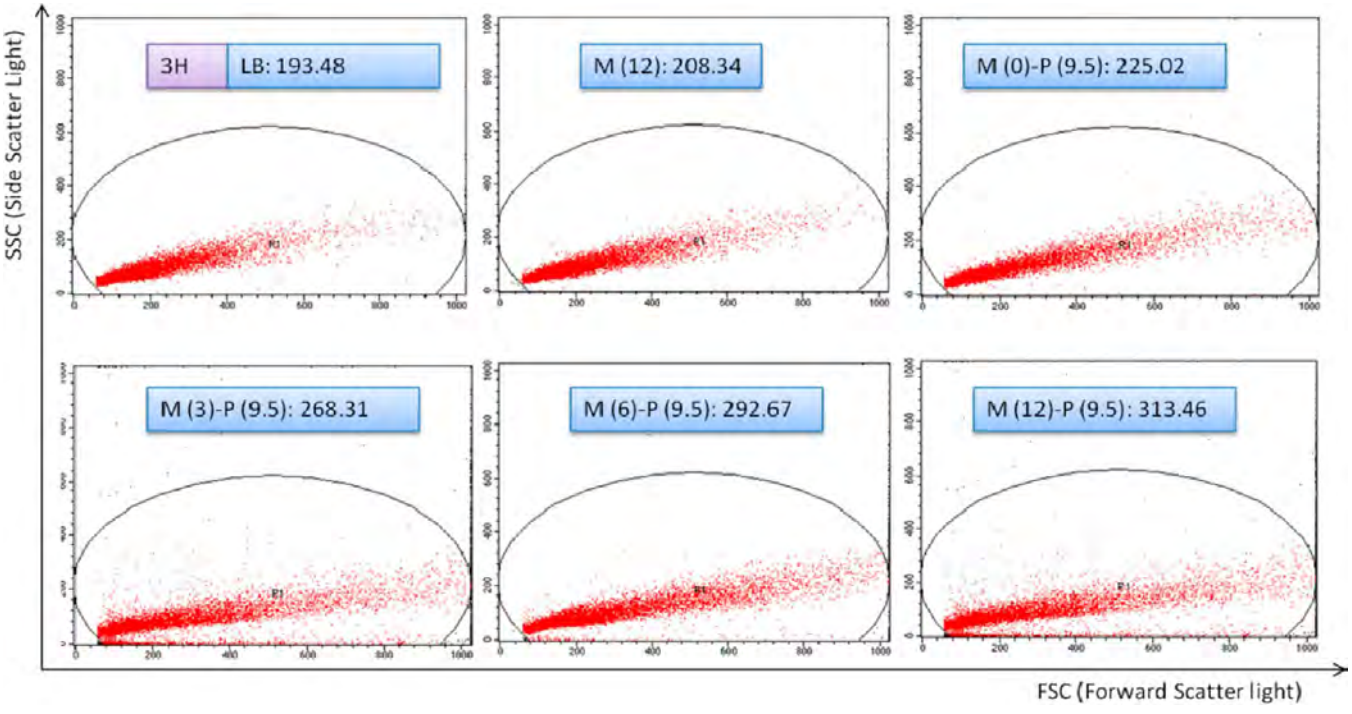

Figure 13. Average cell size of the bacteria in the M(a)-P(9.5) solutions after 3 h. The M(a > 0)-P(9.5) solutions show obvious enlargement in the average cell size.

DOI: 10.1021/acsami.6b02241
ACS Appl. Mater. Interfaces 2016, 8, 9662−9673

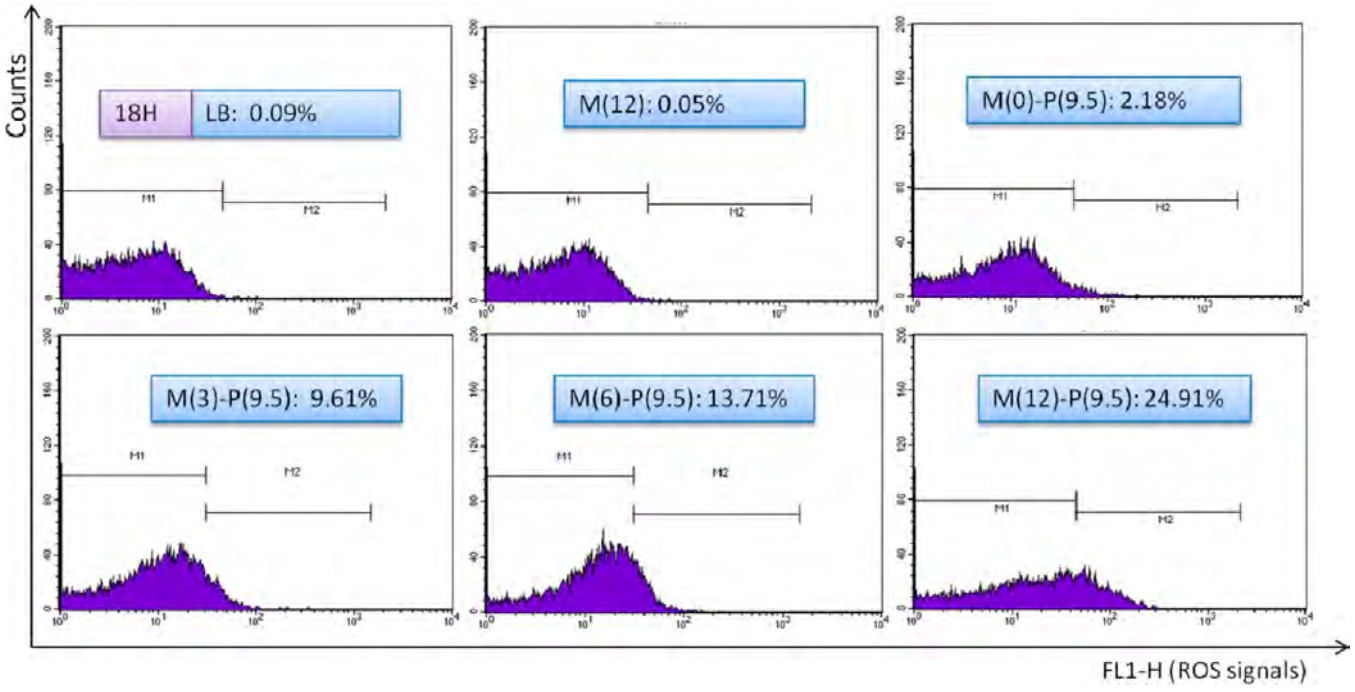

Figure 14. ROS positive bacteria cells in the M(a)-P(9.5) solutions after 18 h. The M(a > 0)-P(9.5) solutions show obvious increase in the ROS positive cells.

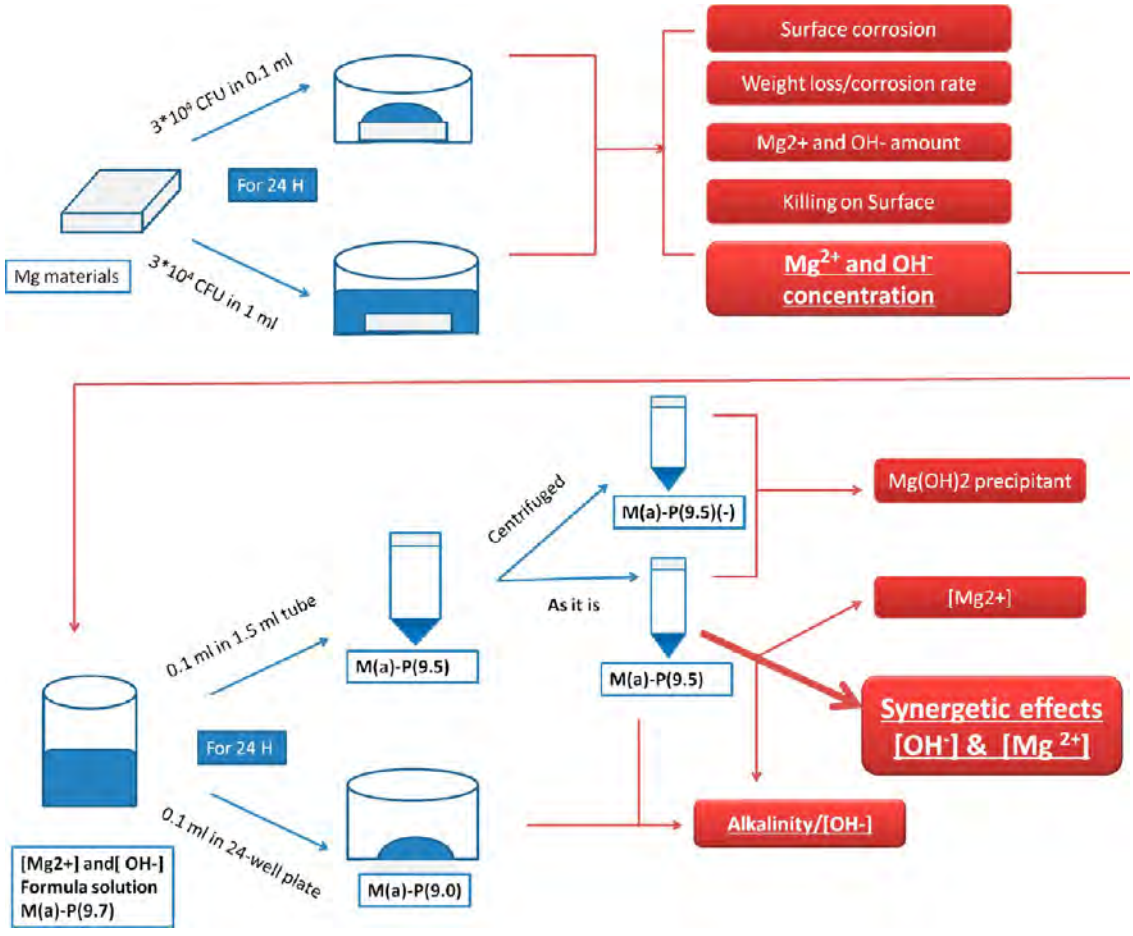

Figure 15. Schematic figure illustrating the (blue) experimental process and (red) evalutation of the various factors affecting the antibacterial properties of Mg. The critical factors are enlarged or underlined.

DOI: 10.1021/acsami.6b02241
ACS Appl. Mater. Interfaces 2016, 8, 9662−9673

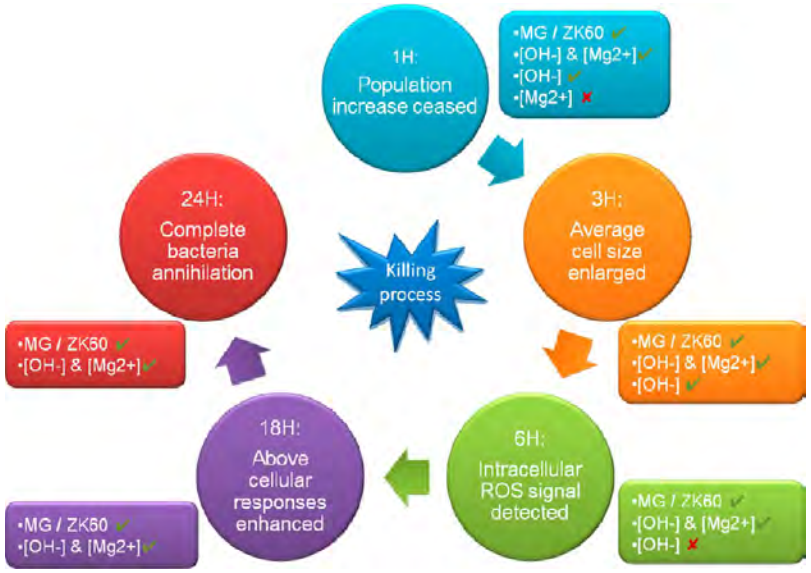

Figure 16. Schematic showing the bacteria killing process and cellular response in 24 h. The treatments that can successfully induce the cellular responses are marked with a check mark, whereas those that cannot are marked with an X and are omitted from the subsequent steps. Only the synergetic effects of alkalinity and magnesium ions can reproduce the whole process as MG and ZK60 do.

experimental investigation for 24 h. A large Mg concentration or $Mg(OH)_2$ precipitate are not dominant factors. Alkalinity may be an important parameter because when the pH diminishes from 9.5 to 9.0, the CFU after 24 h increases by 3 orders of magnitude. However, alkalinity alone cannot account for the antibacterial properties entirely, because the bacteria in M(0)-P(9.5) still undergo exponential growth, as opposed to MG and ZK60 which undergo complete annihilation. However, the M(a > 0)-P(9.5) solutions can effectively prevent the bacteria population from increasing and lead to persistent bacteria death in 24 h. Addition of magnesium ions also reduces the dependence on alkalinity, as the M(a > 0)-P(9.0) solutions also show persistent decline in the bacteria population. The results suggest that the main mechanism is the synergetic effect rendered by both the magnesium ions and alkalinity.

The molecular mechanism of this synergetic effect still needs further exploration. To survive and grow at alkaline pH, bacteria deploy a number of adaptive strategies to keep alkaline pH homeostasis including increased metabolic acid production and higher expression of monovalent cation antiporter.[42] The expressions of TnaA (tryptophan deaminase), TnaB (tryptophan transporter),[43] and Mrp (Na^+/H^+ antiporter)[44] are crucial to bacteria in order to increase intracellular protons in the extracellular alkaline environment. On the other hand, magnesium as a cofactor in many enzymatic reactions and membrane stability promotion is maintained at a very high intracellular concentration compared to many monovalent and divalent ions, ranging between 15 and 30 mM (360−720 ppm) in many cell types.[45,46] Hence, it hardly causes any difference to the bacteria growth at an extracellular concentration of 1200 mg/L such as that used in our experiments. However, when combined with alkalinity, strong bacteria killing ability is achieved. A large concentration of magnesium may activate certain riboswitches, the *cis*-acting RNAs residing within the untranslated regions (UTRs) of mRNAs, which specifically sense small molecule metabolites and as a response, regulate gene expression.[47] Two different classes of riboswitches have been found to function as direct RNA-based genetic sensors of divalent ions and magnesium has been revealed to be the smallest riboswitch ligand.[48] Specifically, the "M-box" riboswitch functioning as an "off" switch in the presence of increased intracellular magnesium, decreasing the expression of downstream genes.[49] This process may impair the expression of the required genes mentioned above in the alkaline environment, thus leading to bacteria inactivation.

The Complete Killing Process in 24 h. Not only can the M(a > 0)-P(9.5) and M(a > 0)-P(9.0) solutions achieve similar CFU reduction like MG and ZK60, but they can also reproduce the killing process at various time points similar to MG and ZK60. As summarized in Figure 16, reduction in the bacteria population commences within 1 h. After 3 h, the average cell size is larger and weak intracellular ROS is detectable. After 6 h, strong intracellular ROS is induced. After 18 h, the ROS positive cells and cell size enlargement are further enhanced and the numbers of remaining bacteria are about one hundred. After 24 h, complete annihilation of bacteria is achieved and no living ones can be detected.

From the perspective of cellular response, oxidative stress is involved in bacteria inactivation. However, intracellular ROS which is not detected immediately emerges several generations (3 h) later. Hence, the oxidative stress is not likely caused by the redox reaction between Mg and H_2O directly but rather a consequence of the combined effects of Mg leaching and alkalinity. Apart from intracellular ROS, the average bacteria cell size becomes larger than that of the control. This suggests that the bacteria have difficulty with normal division and it may be another factor leading to the population reduction besides direct cell death. Alkalinity alone causes certain cell size expansion after 3 h but fails to sustain significant oxidative stress afterward. This may be the reason why bacteria start to proliferate afterward as observed from the experiments.

High Antibacterial Efficiency of Magnesium-Based Materials Compared to Other Biometals. In this study, we used a volume of 0.1 mL which is not usual in Mg antibacterial studies. There are concerns that Mg reacts with H_2O and water evaporation occurs in duration as long as 24 h. However, it is found that the amount of water consumed in the reaction and

DOI: 10.1021/acsami.6b02241
ACS Appl. Mater. Interfaces 2016, 8, 9662−9673

evaporation are not serious if the gaps between the wells are filled with water to prevent loss of the medium by evaporation. In our experiments, as much as 90 μL of the LB medium can be recollected before 6 h, and 50 μL even after 24 h, and so dying from drying does not occur. By adopting this experimental set, we can compare the bacteria killing ability of Mg-based materials and other biometals. Our results show that the antibacterial ability of magnesium is stronger than that of many other biometals such as surface-modified Ti[33,34] or stainless steels[29,30] which only show CFU reduction of less than 3 orders of magnitude. On the contrary, complete annihilation is observed from the two Mg-based materials, and CFU reduction compared to the control is more than 10 orders of magnitude.

CONCLUSION

The inherent antibacterial properties of two Mg-based materials, pure Mg and ZK60 alloy, in 1 and 0.1 mL of the LB medium are investigated. The bacteria are killed more effectively in the solution than on the surface, and the bacteria killing efficiency depends more on the concentrations of the magnesium ions and hydroxyl ions than on the corrosion rate. Formula solutions are made to mimic the killing process and the mechanism involves the combined effects rendered by alkalinity and magnesium ions rather than either of one them or $Mg(OH)_2$ precipitate. Complete annihilation of the initial 3×10^4 bacteria is achieved in 0.1 mL of the LB medium in 24 h, but more than 10^{10} are observed on the control. ROS signals are detected from the bacteria cells but not likely caused by the redox reaction itself, because the ROS signals are detected at least 3 h after the reaction has commenced. Enlargement in the average cell size is also observed during the killing process because the bacteria have difficulty with normal division leading to a smaller bacteria population.

AUTHOR INFORMATION

Corresponding Authors

*E-mail: paul.chu@cityu.edu.hk.
*E-mail: guosonwu@cityu.edu.hk.

Notes

The authors declare no competing financial interest.

ACKNOWLEDGMENTS

This work is supported by Hong Kong Research Grants Council (RGC) General Research Funds (GRF) CityU 112212 and 11301215.

REFERENCES

(1) Bowen, P. K.; McNamara, C. T.; Mills, O. P.; Drelich, J.; Goldman, J. FIB-TEM Study of Magnesium Corrosion Products after 14 Days in the Murine Artery. *ACS Biomater. Sci. Eng.* **2015**, *1* (10), 919−926.

(2) Chen, Y.; Xu, Z.; Smith, C.; Sankar, J. Recent Advances on the Development of Magnesium Alloys for Biodegradable Implants. *Acta Biomater.* **2014**, *10* (11), 4561−4573.

(3) Staiger, M. P.; Pietak, A. M.; Huadmai, J.; Dias, G. Magnesium and Its Alloys as Orthopedic Biomaterials: A Review. *Biomaterials* **2006**, *27* (9), 1728−1734.

(4) Witte, F.; Fischer, J.; Nellesen, J.; Crostack, H. A.; Kaese, V.; Pisch, A.; Beckmann, F.; Windhagen, H. In Vitro and in Vivo Corrosion Measurements of Magnesium Alloys. *Biomaterials* **2006**, *27* (7), 1013−1018.

(5) Xu, L.; Yu, G.; Zhang, E.; Pan, F.; Yang, K. In Vivo Corrosion Behavior of Mg-Mn-Zn Alloy for Bone Implant Application. *J. Biomed. Mater. Res., Part A* **2007**, *83* (3), 703−711.

(6) Zhang, E.; Xu, L.; Yu, G.; Pan, F.; Yang, K. In Vivo Evaluation of Biodegradable Magnesium Alloy Bone Implant in the First 6 Months Implantation. *J. Biomed. Mater. Res., Part A* **2009**, *90* (3), 882−893.

(7) Zhai, Z.; Qu, X.; Li, H.; Yang, K.; Wan, P.; Tan, L.; Ouyang, Z.; Liu, X.; Tian, B.; Xiao, F.; Wang, W.; Jiang, C.; Tang, T.; Fan, Q.; Qin, A.; Dai, K. The Effect of Metallic Magnesium Degradation Products on Osteoclast-Induced Osteolysis and Attenuation of NF-κB and NFATc1 Signaling. *Biomaterials* **2014**, *35* (24), 6299−6310.

(8) Chaya, A.; Yoshizawa, S.; Verdelis, K.; Myers, N.; Costello, B. J.; Chou, D.-T.; Pal, S.; Maiti, S.; Kumta, P. N.; Sfeir, C. In Vivo Study of Magnesium Plate and Screw Degradation and Bone Fracture Healing. *Acta Biomater.* **2015**, *18*, 262−269.

(9) Renvert, S.; Roos-Jansåker, A.-M.; Lindahl, C.; Renvert, H.; Rutger Persson, G. Infection at Titanium Implants with or without a Clinical Diagnosis of Inflammation. *Clin. Oral Implants Res.* **2007**, *18* (4), 509−516.

(10) Mombelli, A.; van Oosten, M. A. C.; Schurch, E.; Land, N. P. The Microbiota Associated with Successful or Failing Osseointegrated Titanium Implants. *Oral Microbiol. Immunol.* **1987**, *2* (4), 145−151.

(11) Fürst, M. M.; Salvi, G. E.; Lang, N. P.; Persson, G. R. Bacterial Colonization Immediately after Installation on Oral Titanium Implants. *Clin. Oral Implants Res.* **2007**, *18* (4), 501−508.

(12) Nandakumar, K.; Sreekumari, K. R.; Kikuchi, Y. Antibacterial Properties of Magnesium Alloy AZ31B: In - Vitro Studies Using the Biofilm-Forming Bacterium Pseudomonas Sp. *Biofouling* **2002**, *18* (2), 129−135.

(13) Robinson, D. a.; Griffith, R. W.; Shechtman, D.; Evans, R. B.; Conzemius, M. G. In Vitro Antibacterial Properties of Magnesium Metal against Escherichia Coli, Pseudomonas Aeruginosa and Staphylococcus Aureus. *Acta Biomater.* **2010**, *6* (5), 1869−1877.

(14) Li, Y.; Liu, G.; Zhai, Z.; Liu, L.; Li, H.; Yang, K.; Tan, L.; Wan, P.; Liu, X.; Ouyang, Z.; Yu, Z.; Tang, T.; Zhu, Z.; Qu, X.; Dai, K. Antibacterial Properties of Magnesium In Vitro and in an In Vivo Model of Implant-Associated Methicillin-Resistant Staphylococcus Aureus Infection. *Antimicrob. Agents Chemother.* **2014**, *58* (12), 7586−7591.

(15) Lock, J. Y.; Wyatt, E.; Upadhyayula, S.; Whall, A.; Nuñez, V.; Vullev, V. I.; Liu, H. Degradation and Antibacterial Properties of Magnesium Alloys in Artificial Urine for Potential Resorbable Ureteral Stent Applications. *J. Biomed. Mater. Res., Part A* **2014**, *102* (3), 781−792.

(16) Witte, F.; Feyerabend, F.; Maier, P.; Fischer, J.; Störmer, M.; Blawert, C.; Dietzel, W.; Hort, N. Biodegradable Magnesium-Hydroxyapatite Metal Matrix Composites. *Biomaterials* **2007**, *28* (13), 2163−2174.

(17) Li, Z.; Gu, X.; Lou, S.; Zheng, Y. The Development of Binary Mg-Ca Alloys for Use as Biodegradable Materials within Bone. *Biomaterials* **2008**, *29* (10), 1329−1344.

(18) Ren, L.; Lin, X.; Tan, L.; Yang, K. Effect of Surface Coating on Antibacterial Behavior of Magnesium Based Metals. *Mater. Lett.* **2011**, *65* (23−24), 3509−3511.

(19) Jamesh, M.; Wu, G.; Zhao, Y.; Chu, P. K. Effects of Silicon Plasma Ion Implantation on Electrochemical Corrosion Behavior of Biodegradable Mg-Y-RE Alloy. *Corros. Sci.* **2013**, *69*, 158−163.

(20) Jin, W.; Wu, G.; Feng, H.; Wang, W.; Zhang, X.; Chu, P. K. Improvement of Corrosion Resistance and Biocompatibility of Rare-Earth WE43 Magnesium Alloy by Neodymium Self-Ion Implantation. *Corros. Sci.* **2015**, *94*, 142−155.

(21) Ryu, H. S.; Hong, S.-H. Corrosion Resistance and Antibacterial Properties of Ag-Containing MAO Coatings on AZ31 Magnesium Alloy Formed by Microarc Oxidation. *J. Electrochem. Soc.* **2010**, *157* (4), C131−C136.

(22) Zhao, Y.; Wu, G.; Jiang, J.; Wong, H. M.; Yeung, K. W. K.; Chu, P. K. Improved Corrosion Resistance and Cytocompatibility of Magnesium Alloy by Two-Stage Cooling in Thermal Treatment. *Corros. Sci.* **2012**, *59*, 360−365.

(23) Wu, G.; Zhao, Y.; Zhang, X.; Ibrahim, J. M.; Chu, P. K. Self-Protection against Corrosion of Aged Magnesium Alloy in Simulated Physiological Environment. *Corros. Sci.* **2013**, *68*, 279−285.

DOI: 10.1021/acsami.6b02241
ACS Appl. Mater. Interfaces 2016, 8, 9662−9673

(24) Qin, H.; Zhao, Y.; An, Z.; Cheng, M.; Wang, Q.; Cheng, T.; Wang, Q.; Wang, J.; Jiang, Y.; Zhang, X.; Yuan, G. Enhanced Antibacterial Properties, Biocompatibility, and Corrosion Resistance of Degradable Mg-Nd-Zn-Zr Alloy. *Biomaterials* **2015**, *53*, 211−220.
(25) Tie, D.; Feyerabend, F.; Müller, W. D.; Schade, R.; Liefeith, K.; Kainer, K. U.; Willumeit, R. Antibacterial Biodegradable Mg-Ag Alloys. *Eur. Cells Mater.* **2013**, *25*, 284−298.
(26) Zhao, Y.; Jamesh, M. I.; Li, W. K.; Wu, G.; Wang, C.; Zheng, Y.; Yeung, K. W. K.; Chu, P. K. Enhanced Antimicrobial Properties, Cytocompatibility, and Corrosion Resistance of Plasma-Modified Biodegradable Magnesium Alloys. *Acta Biomater.* **2014**, *10* (1), 544−556.
(27) He, G.; Wu, Y.; Zhang, Y.; Zhu, Y.; Liu, Y.; Li, N.; Li, M.; Zheng, G.; He, B.; Yin, Q.; Zheng, Y.; Mao, C. Addition of Zn to the Ternary Mg−Ca−Sr Alloys Significantly Improves Their Antibacterial Properties. *J. Mater. Chem. B* **2015**, *3*, 6676−6689.
(28) Song, G.; Atrens, A. Understanding Magnesium Corrosion—A Framework for Improved Alloy Performance. *Adv. Eng. Mater.* **2003**, *5* (12), 837−858.
(29) Bociaga, D.; Komorowski, P.; Batory, D.; Szymanski, W.; Olejnik, A.; Jastrzebski, K.; Jakubowski, W. Silver-Doped Nanocomposite Carbon Coatings (Ag-DLC) for Biomedical Applications − Physiochemical and Biological Evaluation. *Appl. Surf. Sci.* **2015**, *355*, 388−397.
(30) Marciano, F. R.; Bonetti, L. F.; Santos, L. V.; Da-Silva, N. S.; Corat, E. J.; Trava-Airoldi, V. J. Antibacterial Activity of DLC and Ag-DLC Films Produced by PECVD Technique. *Diamond Relat. Mater.* **2009**, *18*, 1010−1014.
(31) Leung, Y. H.; Ng, A. M. C.; Xu, X.; Shen, Z.; Gethings, L. A.; Wong, M. T.; Chan, C. M. N.; Guo, M. Y.; Ng, Y. H.; Djurišić, A. B.; Lee, P. K. H.; Chan, W. K.; Yu, L. H.; Phillips, D. L.; Ma, A. P. Y.; Leung, F. C. C. Mechanisms of Antibacterial Activity of MgO: Non-ROS Mediated Toxicity of MgO Nanoparticles Towards. *Small* **2014**, *10* (6), 1171−1183.
(32) Pan, X.; Wang, Y.; Chen, Z.; Pan, D.; Cheng, Y.; Liu, Z.; Lin, Z.; Guan, X. Investigation of Antibacterial Activity and Related Mechanism of a Series of Nano-Mg(OH)2. *ACS Appl. Mater. Interfaces* **2013**, *5* (3), 1137−1142.
(33) Zhao, Y.; Cao, H.; Qin, H.; Cheng, T.; Qian, S.; Cheng, M.; Peng, X.; Wang, J.; Zhang, Y.; Jin, G.; Zhang, X.; Liu, X.; Chu, P. K. Balancing the Osteogenic and Antibacterial Properties of Titanium by Codoping of Mg and Ag: An in Vitro and in Vivo Study. *ACS Appl. Mater. Interfaces* **2015**, *7* (32), 17826−17836.
(34) Gao, A.; Hang, R.; Huang, X.; Zhao, L.; Zhang, X.; Wang, L.; Tang, B.; Ma, S.; Chu, P. K. The Effects of Titania Nanotubes with Embedded Silver Oxide Nanoparticles on Bacteria and Osteoblasts. *Biomaterials* **2014**, *35* (13), 4223−4235.
(35) Gogniat, G.; Dukan, S. TiO2 Photocatalysis Causes DNA Damage via Fenton Reaction-Generated Hydroxyl Radicals during the Recovery Period. *Appl. Environ. Microbiol.* **2007**, *73* (23), 7740−7743.
(36) Matallana-Surget, S.; Wattiez, R. Impact of Solar Radiation on Gene Expression in Bacteria. *Proteomes* **2013**, *1* (2), 70−86.
(37) Hare, N. J.; Scott, N. E.; Shin, E. H. H.; Connolly, A. M.; Larsen, M. R.; Palmisano, G.; Cordwell, S. J. Proteomics of the Oxidative Stress Response Induced by Hydrogen Peroxide and Paraquat Reveals a Novel AhpC-like Protein in Pseudomonas Aeruginosa. *Proteomics* **2011**, *11* (15), 3056−3069.
(38) Feng, H.; Wang, R.; Sun, P.; Wu, H.; Liu, Q.; Fang, J.; Zhu, W.; Li, F.; Zhang, J. A Study of Eukaryotic Response Mechanisms to Atmospheric Pressure Cold Plasma by Using Saccharomyces Cerevisiae Single Gene Mutants. *Appl. Phys. Lett.* **2010**, *97* (13), 131501.
(39) Dwyer, D. J.; Belenky, P. a; Yang, J. H.; MacDonald, I. C.; Martell, J. D.; Takahashi, N.; Chan, C. T. Y.; Lobritz, M. a; Braff, D.; Schwarz, E. G.; Ye, J. D.; Pati, M.; Vercruysse, M.; Ralifo, P. S.; Allison, K. R.; Khalil, A. S.; Ting, A. Y.; Walker, G. C.; Collins, J. J. Antibiotics Induce Redox-Related Physiological Alterations as Part of Their Lethality. *Proc. Natl. Acad. Sci. U. S. A.* **2014**, *111* (20), E2100−E2109.
(40) von Moos, N.; Slaveykova, V. I. Oxidative Stress Induced by Inorganic Nanoparticles in Bacteria and Aquatic Microalgae–State of the Art and Knowledge Gaps. *Nanotoxicology* **2014**, *8* (6), 605−630.
(41) Moseley, J. B.; Mayeux, A.; Paoletti, A.; Nurse, P. A Spatial Gradient Coordinates Cell Size and Mitotic Entry in Fission Yeast. *Nature* **2009**, *459* (7248), 857−860.
(42) Padan, E.; Bibi, E.; Ito, M.; Krulwich, T. a. Alkaline pH Homeostasis in Bacteria: New Insights. *Biochim. Biophys. Acta, Biomembr.* **2005**, *1717* (2), 67−88.
(43) Richard, H.; Foster, J. W. Escherichia Coli Glutamate- and Arginine-Dependent Acid Resistance Systems Increase Internal pH and Reverse Transmembrane Potential. *J. Bacteriol.* **2004**, *186* (18), 6032−6041.
(44) Kosono, S.; Asai, K.; Sadaie, Y.; Kudo, T. Altered Gene Expression in the Transition Phase by Disruption of a Na+/H+ Antiporter Gene (shaA) in Bacillus Subtilis. *FEMS Microbiol. Lett.* **2004**, *232* (1), 93−99.
(45) Wolf, F. I.; Cittadini, A. Chemistry and Biochemistry of Magnesium. *Mol. Aspects Med.* **2003**, *24* (1−3), 3−9.
(46) Wolf, F. I.; Torsello, A.; Fasanella, S.; Cittadini, A. Cell Physiology of Magnesium. *Mol. Aspects Med.* **2003**, *24* (1−3), 11−26.
(47) Ramesh, A.; Winkler, W. C. Magnesium-Sensing Riboswitches in Bacteria. *RNA Biol.* **2010**, *7* (1), 77−83.
(48) Cromie, M. J.; Shi, Y.; Latifi, T.; Groisman, E. a. An RNA Sensor for Intracellular Mg2+. *Cell* **2006**, *125* (1), 71−84.
(49) Dann, C. E.; Wakeman, C. a.; Sieling, C. L.; Baker, S. C.; Irnov, I.; Winkler, W. C. Structure and Mechanism of a Metal-Sensing Regulatory RNA. *Cell* **2007**, *130* (5), 878−892.

DOI: 10.1021/acsami.6b02241
ACS Appl. Mater. Interfaces 2016, 8, 9662−9673